J.Serb.Chem.Soc. 68(11)849–857(2003)
JSCS – 3106

UDC 547.291+542.943:54–44+546.226–323
Original scientific paper

Comparison of formic acid oxidation at supported Pt catalyst and at low-index Pt single crystal electrodes in sulfuric acid solution

AMALIJA V. TRIPKOVIĆ, KSENIJA DJ. POPOVIĆ and JELENA D. LOVIĆ

ICTM – Center for Electrochemistry, University of Belgrade, Njegoševa 12, P. O. Box 473, 11001 Belgrade, Serbia and Montenegro

(Received 4 April, revised 9 July 2003)

Abstract: The oxidation of formic acid was studied at supported Pt catalyst (47.5 wt%. Pt) and a low-index single crystal electrodes in sulfuric acid. The supported Pt catalyst was characterized by the TEM and HRTEM techniques. The mean Pt particle diameter, calculated from electrochemical measurements, fits well with Pt particle size distribution determined by HRTEM. For the mean particle diameter the surface averaged distribution of low-index single crystal facets was established. Comparison of the activities obtained at Pt supported catalyst and low-index Pt single crystal electrodes revealed that Pt(111) plane is the most active in the potential region relevant for fuel cell applications.

Keywords: formic acid oxidation, Pt single crystals, supported Pt catalyst, particle size, surface distribution of crystallographic sites.

INTRODUCTION

Simple organic compounds, such as methanol, formaldehyde and formic acid have been extensively studied as fuels for fuel cells. Formic acid is relatively benign and non-explosive which makes it facile in handling and distribution, as compared to hydrogen. On the other hand, it has a lower energy content with respect to hydrogen or methanol. Recent data have shown, however, that formic acid fuel cells are attractive alternatives for small portable fuel cell applications.[1]

In contrast to the limited informations on formic acid properties as a fuel, many results have been reported concerning electrocatalytic oxidation of formic acid from the fundamental viewpoint. Formic acid was studied on polycrystalline[2] and single crystal Pt electrodes.[3–7] There is an agreement that platinum is initially a good catalyst, but the metal surface is rapidly poisoned by the strongly adsorbed intermediates identified by spectroscopic studies.[8,9]

The efforts have been made to enhance oxidation rates of formic acid on platinum by adding a variety of surface modifiers (adatoms). The increase in the reactivity induced by adatoms has been accounted for by a "third body effect", *i.e.*, the third body prevents poison to form on the surface.[10–13]

Despite the simplicity of the formic acid oxidation with only two electrons involved, the reaction proceeds through two parallel paths on platinum[14] leading to direct formation of CO_2 and to the formation of CO_{ad}, which poisons the electrode surface. Both paths are structure sensitive.[15]

There are only a few papers reported so far dealing with formic acid oxidation on Pt-based nanoparticle catalyst,[16,17] *i.e.*, on the high surface area catalysts for anode application in the direct oxidation formic acid fuel cells.

However, the problem with CO poisoning at potentials relevant for fuel cells remains still open as in a case of methanol oxidation.

The present paper aims to examine the electrocatalytic properties of supported Pt catalyst (47.5 wt% Pt) in electrochemical oxidation of formic acid in sulfuric acid solution and to compare the results with the data obtained at low-index single crystal platinum electrodes. This approach was based on the TEM, HRTEM and electrochemical measurements, which allowed the correlation between the size of Pt nanoparticles and the surface distribution of (111), (100) oriented facets and low-coordinated (110) edge and corner sites.

EXPERIMENTAL

Commercially available Pt-based catalyst (47.5 wt% Pt) provided by Tanaka Precious Metals Group supported on high surface area carbon was used. The catalyst was characterized by the transmission electron microscopy (TEM) and by high resolution transmission electron microscopy (HRTEM) techniques. TEM and HRTEM images of the electrode as well as the histogram of the particle size distribution are shown in Fig. 1 (a –c). TEM analysis (a) shows that the distribution of metal particle on the carbon support is reasonably uniform. Typical highly faceted cubooctahedral nanoparticles are shown in part (b). The histogram of the particle size distribution (c) reveals that the average particle size is ranged between 2 nm and 6 nm.

The catalytic acitivty of the catalyst was determined by using the thin-film rotating disk (RDE) method. The catalyst was ultrasonically dispersed in Millipore water and a drop of this suspension was placed onto a polished glassy carbon disk (Sigradur G) diameter 6.7 mm, resulting in metal loading of 20 μg cm^{-2}. After drying in nitrogen at room temperature, the deposited catalyst layer was covered with 20 μl of a diluted aques Nafion solution leading to thickness of ≈ 0.2 μm. Finally, the electrode was immersed in nitrogen purged electrolyte.

In order to verify that the Nafion film used to attach the catalyst particles onto the glassy carbon RDE does not impose additional film diffusion resistance the polarization curves for the hydrogen oxidation reaction, (HOR), in a solution saturated with H_2 were recorded on supported Pt catalyst in sulfuric acid solution (Fig. 2). The Levich-Koutecky plot inferred from the diffusion limiting currents at 0.3 V is shown as an inset in Fig. 2.

As the value of $B\ c_0 = 6.51 \times 10^{-2}$ mA cm^{-2} $rpm^{-1/2}$ closely agrees with the theoretical value of 6.54×10^{-2} mA cm^{-2} $rpm^{-1/2}$, assumed from the Levich equation:

$$j_0 = 0.62\, nFD^{2/3}\, \nu^{-1/6}\, c_0\omega^{1/2} = B\, c_0\, \omega^{1/2} \qquad (1)$$

it appears that there is no significant mass transfer resistance through the Nafion film.

The catalytic activity was measured either by recording the potentiodynamic (sweep rate 50 mV s^{-1}) or quasi steady-state (sweep rate 1 mV s^{-1}) polarization curves.

Formic acid (Merck, p.a.) was added to the solution while the electrode was held at ≈ 0.05 V. The reference electrode was a saturated calomel electrode (SCE). All potentials are referred to the reversible hydrogen electrode (RHE) in the same electrolyte. Current densities in Figs. 3 – 6 are given on real surface

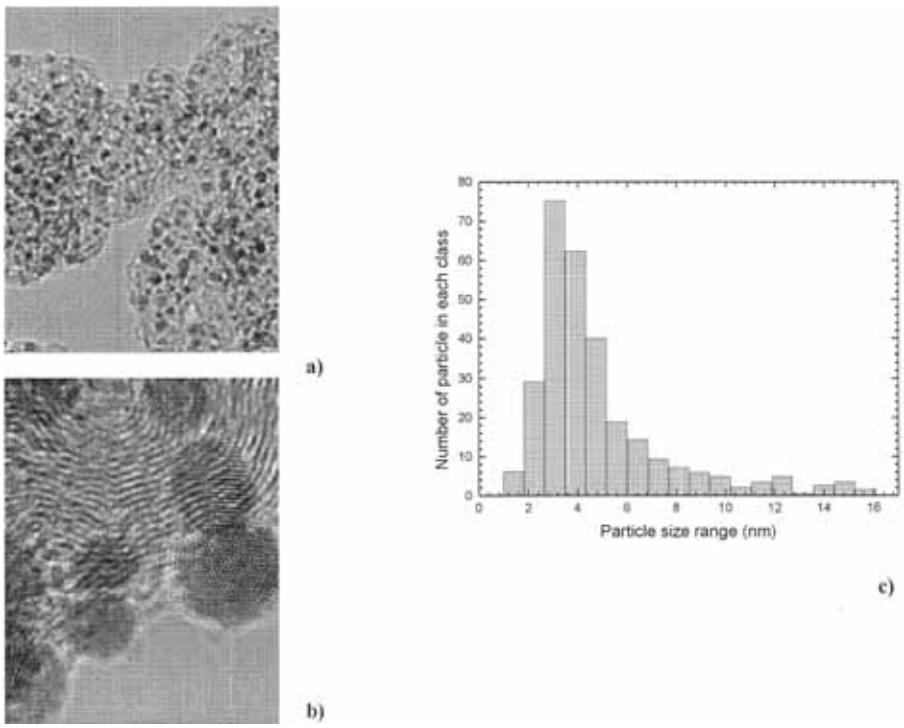

Fig. 1. TEM image of Pt nanoparticles on a carbon black support (a); HRTEM image of generally facetted shapes of nanoparicles (b); particle size distribution (c).

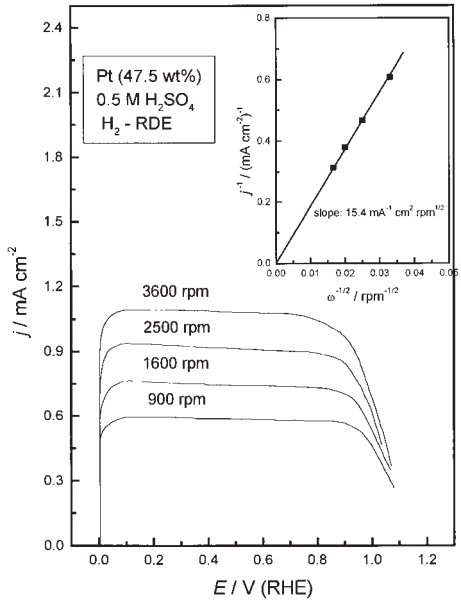

Fig. 2. Polarization curves for the HOR on Pt supported catalyst in 0.5 M H_2SO_4. Inset: plot of $1/j$ *vs.* $\omega^{-1/2}$.

area scale.

RESULTS AND DISCUSSION

Basic voltammograms

Figure 3 illustrates the voltammograms of the supported Pt catalyst (a) and low-index single crystal Pt electrodes (b), (only hydrogen adsorption/desorption region), in sulfuric acid solution. The potential region of hydrogen adsorption/desorption on supported Pt catalyst accompanied with bisulfate desorption/adsorption is separated from the reversible/irreversible oxide formation by the double layer potential region. The features in the hydrogen region could be rationalized on the basis of hydrogen electrochemistry at low-index single crystal platinum electrodes in the same acidic solution. The H-desorption peak at $E \approx 0.15$ V can be correlated with the Pt(110) sites. The more positive H-desorption peaks at $E \approx 0.3$ V suggests the presence of Pt(100) related facets. The broad and featureless H-desorption occurring over the potential range $0.05 \text{ V} < E < 0.35$ V, below the Pt(110) and Pt(100) peaks, indicates the presence of Pt (111) correlated sites. This

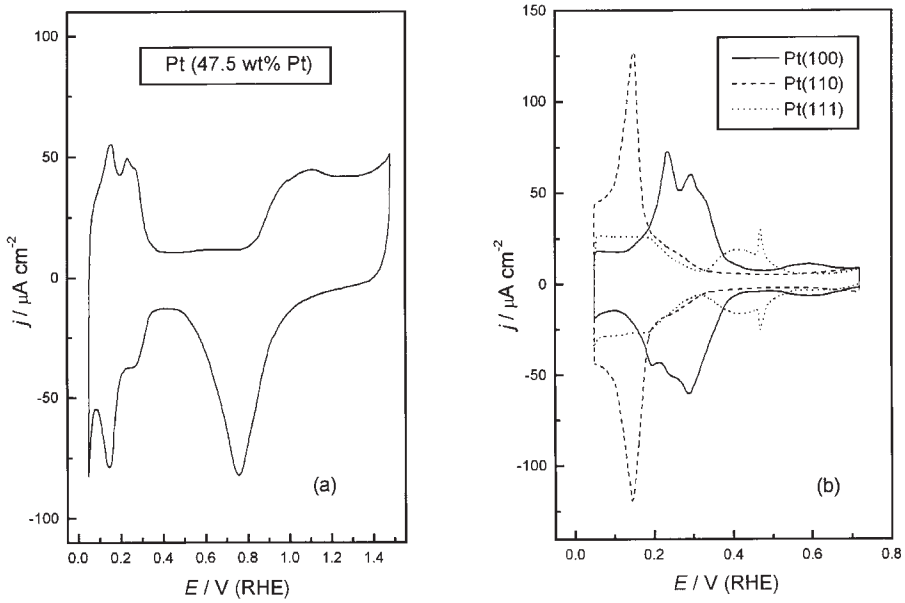

Fig. 3. Cyclic voltammograms for Pt supported catalyst (a) and Pt low-index single crystal electrodes (b) in 0.5 M H_2SO_4. $\nu = 50$ mV s^{-1}; $T = 295$ K.

observation is consistent with the fact that the nanostructured platinum was composed of low coordination – number single crystals.[18]

Basic voltammogram for supported catalyst (a) was used for an estimation of the real surface area (S), mass specific surface area (S_1) and diameter of Pt particles (d).

The hydrogen adsorption charge (Q_H) in the potential region $0.05 \text{ V} < E < 0.4$ V was

determined as $Q_H = 0.5(Q_{total} - Q_{DL})$, where Q_{total} is a total charge transfer in the hydrogen adsorption/desorption region and Q_{DL} is a capacitive charge from both double layer charging and a capacitance of the high surface area carbon support. Assuming that $Q_H = 0.21$ mC cm^{-2} corresponds to a monolayer of adsorb hydrogen[19] the value for real surface area is estimated as $S = 4.6$ cm^2. This value normalized by mass of Pt gives mass specific surface area $S_1 = 66$ m^2 g^{-1}. Assuming that the Pt particles are spherical the partials diameter calculated by using the equation $d = 6\times10^3/\rho S_1$, where $\rho = 21.4$ g cm^{-3} and S_1 is mass specific surface area is $d = 4.3$ nm. This value fits well with particle size distribution obtained by HRTEM.

Formic acid oxidation

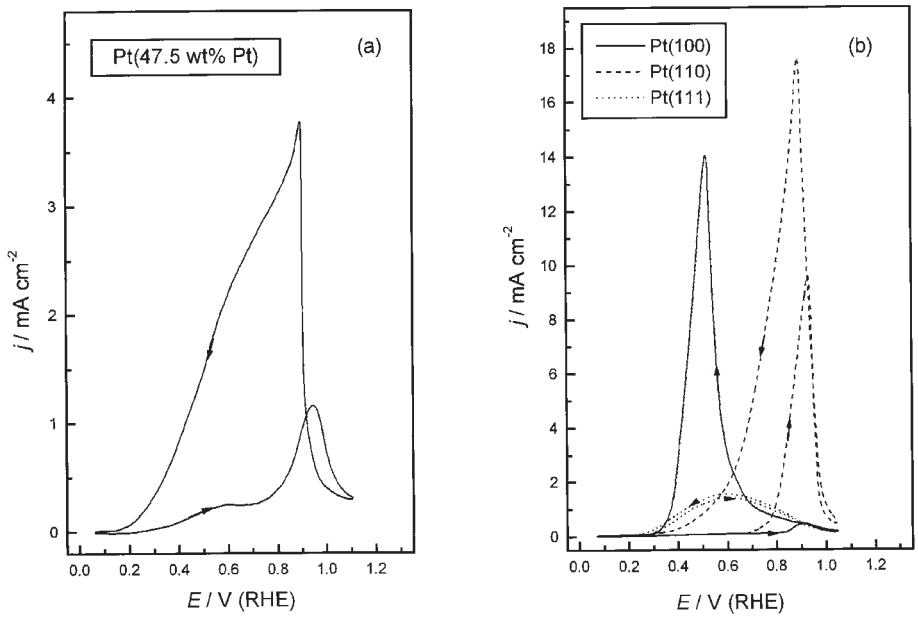

Fig. 4. Cyclic voltammograms for the oxidation of 0.5 HCOOH on Pt supported catalyst (a) and on Pt low-index single crystal electrodes (b) in 0.5 M H_2SO_4. $\nu = 50$ mV s^{-1}; $T = 295$ K.

Potentiodynamic measurements. The polarization curves for formic acid oxidation on supported Pt (a) and a low-index platinum electrodes are presented in Fig. 4 (a and b, respectively).

The fraction commences at the surface still partially covered by H_{ad} species and proceeds further through the double layer region with a relatively slow kinetics. Then it becomes faster in the potential region related to the adsorption of oxygen-containing species, giving a current maximum at $E \approx 0.95$ V. Upon sweep reversal an increase of the activity is seen which is followed by a gradual decrease as the overpotentials decrease.

The polarization curve for formic acid oxidation on supported Pt catalyst has similar shape as the curve obtained on a polycrystalline Pt bulk electrode[2] suggesting that there is

no unexpected surface composition of the nanoparticles compared with a bulk electrode.

A brief interpretation of the voltammograms given in Fig. 4b shows that both Pt (110) and Pt (100) are completely blocked with poisoning species during the positive sweep up to high potentials where these species can be oxidized. Upon reversal of the sweeps, the reaction attains high rates on both planes. On the contrary, the Pt (111) surface shows a negligible poisoning effect over the whole potential region where the reaction occurs. This observation is supported by the almost overlapping of the sweeps recorded in both directions of potential scanning.

By comparing the shape of voltammograms on the Pt(*hkl*) electrodes and on supported Pt catalyst, it could be suggested that formic acid is oxidized predominantly at the (111) oriented sites up to $E \approx 0.7$ V, in the positive going sweep, while the peak of $E \approx 0.95$ V, as well as the large increase of the currents in the negative direction correspond to oxidation at the (110) and (100) facets.

This interpretation is supported by the relationship between Pt particle size and the different surface sites (crystal facets, edges, corners) done by Kinoshita[20,21] on the basis of the theoretical analysis of ideal geometric structures, which are representative of small Pt particles. The space lattice of platinum is face-centered cubic and Pt particles are generally represented as cubooctahedral structures consisting of Pt atoms arranged in (111) and (100) crystallographic faces bounded by edge and corner atoms. The concentration of surface atoms at the different crystallographic sites vary with the change of particle size. For an average Pt particle diameter of 4.3 nm, calculated in this work, the surface-averaged distribution amounts: ≈ 65 % (111) sites, ≈13 % (100) sites and 22 % corner and edge sites (which may be correlated with (110) sites).

The data given in Table I displaying the activities of Pt supported catalyst and single crystal Pt electrodes at $E = 0.5$ V show that supported Pt catalyst is more active than both the Pt(100) and the Pt(110) electrodes but less active than the Pt(111) electrode.

In order to obtain a better understanding of formic acid oxidation, the reaction is studied from its early stage to the potentials of interest for electrocatalysis.

Figure 5 shows the onset of formic acid oxidation in sulfuric acid and the basic voltammogram for supported Pt catalyst (a). The reaction commences in the hydrogen adsorption/desorption region at $E \approx 0.15$ V and, in the case of sulfuric acid, the onset of the reaction could not be associated with OH^- anions adsorption.

The first sweep up to $E = 0.55$ V (b) shows an increase of the specific current density with potential and its decrease upon reversal of the scan. The decrease of the oxidation currents in the second sweep compared with those recorded in the first sweep indicates a poisoning effect. This surface blocking is caused by the presence of (110) and (100) oriented sites which are very sensitive to "poison" adsorption.

Upon sweep reversal at $E = 0.75$ V (c) a small hysteresis in the oxidation currents occurs with some increased activity observed during the negative going sweep. This feature remains unchanged during further scanning suggesting the absence of a poisoning effect. Actually, it means that the some poison formed in the reaction can be oxidized up to $E =$

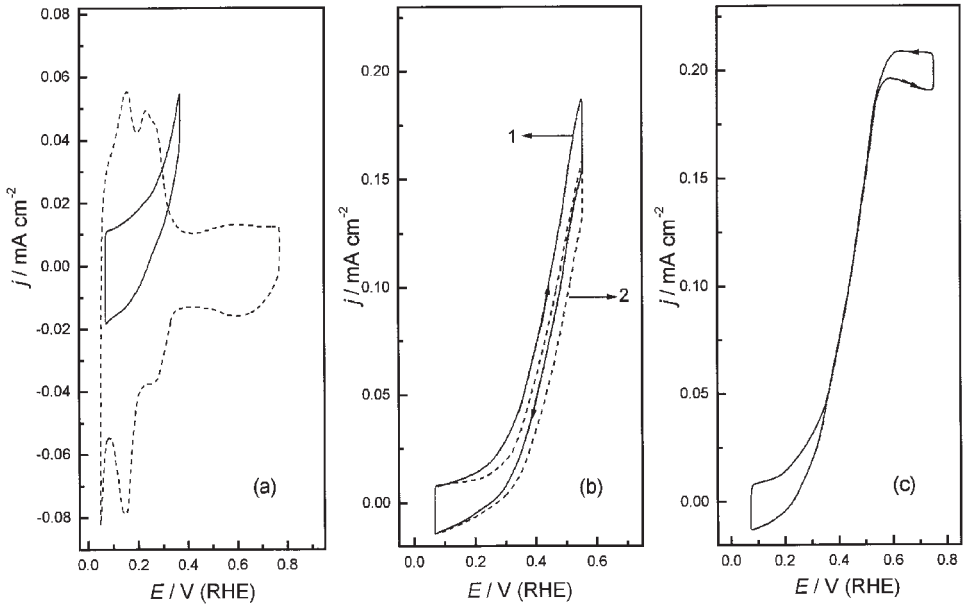

Fig. 5. Cyclic voltammogram for the oxidation of 0.5 M HCOOH up to different positive potential limits on a Pt supported catalyst in 0.5 M H_2SO_4. $\nu = 50$ mV s^{-1}; $T = 295$ K.

0.75 V. Most likely CO_{ad} is the dominant poison which cannot be removed from the nanostructured Pt catalyst until the potential exceeds at least 0.5 V while a sharp peak is seen at 0.76 V.[22]

From the viewpoint of the participation in the reaction of different oriented facets in the supported Pt catalyst it could be suggested that in the potential region up to $E = 0.75$ V the reaction takes place predominantly at the (111) oriented facets although the influence of (110) and (100) oriented sites could not be neglected.

TABLE I. Activities of Pt supported catalyst and Pt single crystal electrodes at $E = 0.5$ V

	Pt (47.5 wt% Pt)	Pt(111)	Pt(100)	Pt(110)
j / mA cm^{-2}	0.186	1.18	0.08	0.08

Quasi steady-state measurements. The quasi steady-state curve obtained in formic acid oxidation on supported Pt catalyst is given in Fig. 6.

The reaction follows a Tafel type equation in the potential region between 0.25 V and 0.55 V giving a well defined Tafel line with the slope ≈ 120 mV/dec. It should be pointed out that in this potential region formic acid oxidation takes place predominantly at the (111) oriented facets. This suggestion is confirmed by the quasi steady state curve for formic acid oxidation at the Pt(111) plane shown in the inset of Fig. 6, which has the same slope of ≈ 120 mV/dec in almost the same potential region. The Pt(111) electrode is also more active than supported Pt catalyst under the quasi steady-state conditions although less

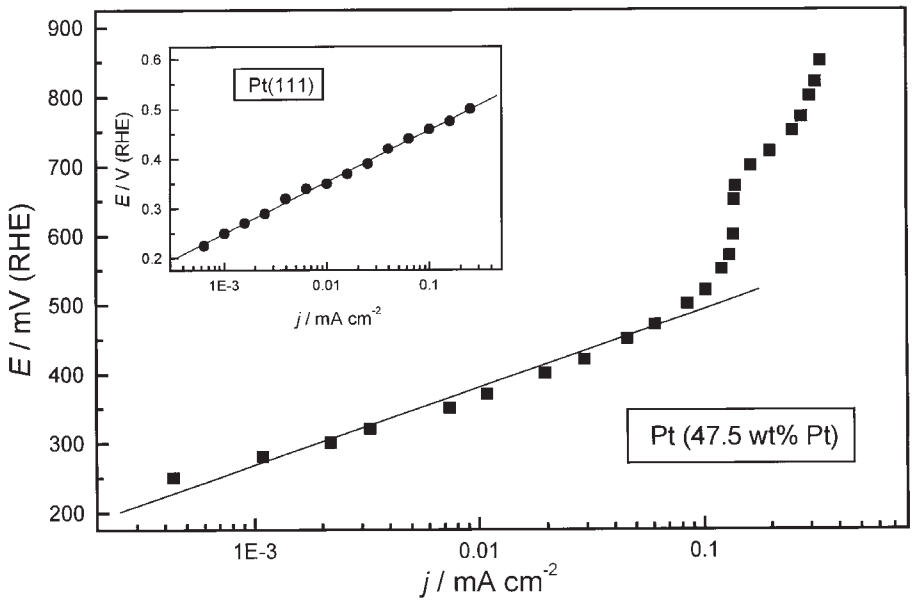

Fig. 6. Tafel plots for the oxidation of 0.5 M HCOOH in 0.5 M H_2SO_4 on Pt supported catalyst and on a Pt(111) surface (inset). $\nu = 1$ mV s^{-1}; $T = 295$ K.

pronounced compared with potentiodynamic conditions (Table I). At $E = 0.5$ V low-index (111) surface, in respect to supported Pt catalyst, is 3 times more active in steady-state measurements and 6 times in potentiodynamic measurements. It is an evidence that the true catalytic activity can be obtained only in steady-state measurements, while the activities observed in potentiodynamic experiments are transient in nature.

CONCLUSIONS

1. TEM and HRTEM analysis of supported Pt catalyst (47.5 wt % Pt) used have shown:

– a relatively uniform distribution of Pt nanoparticles on the carbon support

– cubooctahedral shape of the Pt nanoparticles

– an average Pt particle size between 2 nm and 6 nm.

2. The mean particle diameter $d = 4.3$ nm calculated in this work is in a good agreement with a particle size distribution determined by HRTEM.

3. For the mean particle diameter of 4.3 nm, the surface distribution amounts: 65 % (111) sites, 13 % (100) sites and 22 % corner and edge sites (which may be correlated with low coordination (110) sites.

4. Supported Pt catalyst is more active than (100) and (110) surfaces, but significantly less active than (111) surface in the potential region relevant for electrocatalytic consideration.

Acknowledgement: The authors are grateful to Dr. Nenad Marković for the TEM and HRTEM images,

obtained in the National Center for Electron Microscopy, Lawrence Berkeley National Laboratory, Berkeley. This work was supported by the Ministry of Science, Technology and Development of Serbia, Contract No. H-1796.

ИЗВОД

ПОРЕЂЕЊЕ ОКСИДАЦИЈЕ МРАВЉЕ КИСЕЛИНЕ НА Pt КАТАЛИЗАТОРУ НА НОСАЧУ И НА НИСКОИНДЕКСНИМ Pt МОНОКРИСТАЛИМА У СУМПОРНОЈ КИСЕЛИНИ

АМАЛИЈА В. ТРИПКОВИЋ, КСЕНИЈА Ђ. ПОПОВИЋ и ЈЕЛЕНА Д. ЛОВИЋ

ИХТМ – Центар за електрохемију, Универзитет у Београду, Његошева 12, п. пр. 473, 11000 Београд

Оксидација мравље киселине испитивана је на Pt катализатору нанетом на активни угаљ (47,5 мас % Pt) и на ниско-индексним Pt монокристалним електродама у сумпорној киселини. Први катализатор је окарактерисан коришћењем техника трансмисионе електронске микроскопије ниске (TEM) и високе резолуције (HRTEM), при чему је одређена дистрибуција, величина и облик наночестица Pt. Средњи пречник наночестица, израчунат из електрохемијских мерења, сагласан је расподели величина честица добијеној HRTEM анализом. На основу средњег пречника наночестица дата је просечна дистрибуција (111), (100) и (110) места на површини катализатора на носачу. Овај катализатор је активнији у оксидацији мравље киселине од монокристалних Pt електрода оријентације (100) и (110), али је мање активан од Pt(111) електроде у области потенцијала релевантној за примену у горивном спрегу.

(Примљено 4. априла, ревидирано 9. јула 2003)

REFERENCES

1. M. Weber, J. T. Wang, S. Wasmus, R. F. Savinell, *J. Electrochem. Soc.* **143** (1996) L158
2. A. Capon, R. Parsons, *J. Electroanal. Chem. Interfacial Electrochem.* **44** (1973) 1
R. R. Adžić, A. V. Tripković, W. O'Grady, *Nature* **296** (1982) 137
4. A. Tripković, K. Popović, R. R. Adžić, *J. Chim. Phys.* **88** (1991) 1635
5. J. Clavilier, R. Parsons, R. Durand, C. Lamy, J. M. Leger, *J. Electroanal. Chem. Interfacial Electrochem.* **124** (1981) 321
6. C. Lamy, J. M. Leger, *J. Chim. Phys. – Chim. Biol.* **88** (1991) 1649
7. T. Iwasita, X. H. Xia, E. Herrero, H. D. Liess, *Langmuir* **12** (1996) 4260
8. A. Bewick, K. Kunimatsu, B. S. Pons, *J. Electroanal. Chem.* **160** (1984) 147
9. B. Beden, F. Hahn, S. Juanto, C. Lamy, J. M. Leger, *J. Electroanal. Chem.* **225** (1987) 215
10. M. Watanabe, M. Horiuchi, S. Moto, *J. Electroanal. Chem. Interfacial Electrochem.* **250** (1988) 117
11. M. D. Macia, E. Herrero, J. M. Feliu, A. Aldaz, *J. Electroanal. Chem.* **500** (2001) 498
12. H. A. Gasteiger, N. Marković, P. N. Ross Jr., E. J. Cairns, *Electrochim. Acta* **39** (1994) 1825
13. R. R. Adžić, A. V. Tripković, N. M. Marković, *J. Electroanal. Chem.* **150** (1983) 79
14. R. Parsons, T. Van der Noot, *J. Electroanal. Chem.* **257** (1988) 9
15. C. Lamy, J. M. Leger, C. Clavilier, R. Parsons, *J. Electroanal. Chem.* **150** (1983) 71
16. N. M. Marković, H. A. Gasteiger, P. N. Ross Jr, X. Jiang, I. Villegas, M. J. Weaver, *Electrochim. Acta.* **40** (1995) 91
17. V. Climent, E. Herrero, J. M. Feliu, *Electrochim. Acta* **44** (1988) 1403
18. P. Stonehart, *J. Appl. Electrochem.* **22** (1992) 995
19. B. B. Damaskin, D. A. Petrii, V. V. Batrakov, *Adsorption of Organic Compound on Electrodes*, Plenum Press, New York, London, 1971
20. K. Kinoshita, *J. Electrochem. Soc.* **137** (1990) 845
21. K. Kinoshita, *Electrochemical Oxygen Technology*, Wiley, New York, 1992

22. J. Jiang, A. Kucernak, *J. Electroanal. Chem.* **520** (2002) 64.